The Astrophysical Journal, 687:50–58, 2008 November 1

EXPLORING THE EVOLUTIONARY PATHS OF THE MOST MASSIVE GALAXIES SINCE $z \sim 2$

Pablo G. Pérez-González,[1,2] Ignacio Trujillo,[3] Guillermo Barro,[1] Jesús Gallego,[1]
Jaime Zamorano,[1] and Christopher J. Conselice[4]
Received 2008 May 15; accepted 2008 July 7

ABSTRACT

We use *Spitzer* MIPS data from the FIDEL Legacy Project in the extended Groth strip to analyze the stellar mass assembly of massive ($M > 10^{11}\ M_{\odot}$) galaxies at $z < 2$ as a function of structural parameters. We find 24 μm emission for more than 85% of the massive galaxies morphologically classified as disks, and for more than 57% of the massive systems morphologically classified as spheroids at any redshift, with about 8% of sources harboring a bright X-ray- and/or infrared-emitting AGN. More noticeably, ~60% of all compact massive galaxies at $z = 1$–2 are detected at 24 μm, even when rest-frame optical colors reveal that they are dead and evolving passively. For spheroid-like galaxies at a given stellar mass, the sizes of MIPS nondetections are smaller by a factor of ~1.2 in comparison with IR-bright sources. We find that disklike massive galaxies present specific SFRs ranging from 0.04 to 0.2 Gyr^{-1} at $z < 1$ (SFRs ranging from 1 to 10 $M_{\odot}$ yr^{-1}), typically a factor of 3–6 higher than massive spheroid-like objects in the same redshift range. At $z > 1$, and more pronouncedly at $z > 1.3$, the median specific SFRs of the disks and spheroids detected by MIPS are very similar, ranging from 0.1 to 1 Gyr^{-1} (SFR = 10–200 $M_{\odot}$ yr^{-1}). We estimate that massive spheroid-like galaxies may have doubled (at the most) their stellar mass from star-forming events at $z < 2$: less than 20% mass increase at $1.7 < z < 2.0$, up to 40% more at $1.1 < z < 1.7$, and less than 20% additional increase at $z < 1$. Disklike galaxies may have tripled (at the most) their stellar mass at $z < 2$ from star formation alone: up to ~40% mass increase at $1.7 < z < 2.0$, and less than 180% additional increase below $z = 1.7$ occurred at a steady rate.

Subject headings: galaxies: elliptical and lenticular, cD — galaxies: evolution — galaxies: formation — galaxies: high-redshift — galaxies: photometry — galaxies: spiral — galaxies: starburst — infrared: galaxies

1. INTRODUCTION

The formation and evolution of massive ($M > 10^{11}\ M_{\odot}$) galaxies is one of the most studied topics in extragalactic astronomy during the last decade. Early expectations from hierarchical galaxy formation models considered that star formation began in low-mass systems which built more massive galaxies through sequential merging (Baugh et al. 1996; Cole et al. 2000), in a process similar to the growth of structures in cold dark matter simulations (Springel et al. 2005). In apparent contradiction with hierarchical assembly, the finding of a substantial population of massive galaxies at $z > 1$ (Elston et al. 1988; Hughes et al. 1998; Franx et al. 2003; Glazebrook et al. 2004), some of them containing old stellar populations and evolving passively (according to their red optical colors: Daddi et al. 2004; Reddy et al. 2005; and spectra: Kriek et al. 2006, 2008; Cimatti et al. 2008), seems to favor a downsizing formation scenario (Cowie et al. 1996; Heavens et al. 2004; Juneau et al. 2005; Pérez-González et al. 2005; Bundy et al. 2006). This population of $z > 1$ massive galaxies accounts for a significant fraction of the local stellar mass density (~20% as early as $z \sim 2$, and ~10% at $z \sim 4$: Fontana et al. 2006; Arnouts et al. 2007; Pérez-González et al. 2008). The discovery of such a population reinforced the idea that both stars and their host galaxies are coeval (resembling a monolithic-like collapse), and consequently, no expectations of structure evolution in these galaxies should be expected. For this reason, the recent observational evidence showing that the most massive galaxies were much more compact in the past (Daddi et al. 2005; Trujillo et al. 2006; Longhetti et al. 2007; Cimatti et al. 2008) has been surprising, and has again opened the question of how the stellar populations of these galaxies were assembled into their present shape.

The size evolution of the most massive objects since $z \sim 2$ has been characterized by Trujillo et al. (2007). These authors found that, at a given stellar mass, disklike objects at $z \sim 1.5$ were a factor of 2 smaller than their present-day counterparts. For spheroid-like objects, the evolution has been even stronger: they were a factor of 4 smaller at $z \sim 1.5$ than nearby similar mass ellipticals. In addition, the stellar mass densities of these high-z galaxies were almost 2 orders of magnitude higher than objects of the same mass today. These superdense galaxies have been found at even higher ($z \sim 2.5$) redshifts (Zirm et al. 2007; Toft et al. 2007; van Dokkum et al. 2008), adding more controversy to the debate about the formation and evolution of massive galaxies.

Two processes have been proposed to allow the superdense high-z galaxies to migrate to the local stellar mass–size relation. The first process is dissipationless (with absence of star formation) merging. Given the high metal abundances and old ages of the stellar population present in local massive elliptical galaxies (e.g., Gallazzi et al. 2006; Sánchez-Blázquez et al. 2006; Jimenez et al. 2007), these mergers should preferentially be dry (De Lucia et al. 2006), and occur between $z \sim 1.5$ and $z = 0$, the epoch when the red sequence appears (Labbé et al. 2007). In this context, a particular effective size evolutionary mechanism ($r_e \sim M^{1.3}$) has been provided by Boylan-Kolchin et al. (2006) through head-on mergers of galaxies. The second possibility is the smooth envelope accretion scenario (Naab et al. 2007), where accreted

[1] Departamento de Astrofísica, Facultad de CC. Físicas, Universidad Complutense de Madrid, E-28040 Madrid, Spain.
[2] Associate Astronomer at Steward Observatory, University of Arizona.
[3] Instituto de Astrofísica de Canarias, Vía Láctea s/n, E-38200 La Laguna, Tenerife, Spain.
[4] School of Physics and Astronomy, University of Nottingham, Nottingham NG7 2RD, UK.

stars (mainly provided by minor mergers) form an envelope whose size increases smoothly at decreasing redshift.

The goal of this paper is to explore the evolutionary paths followed by the most massive galaxies and their dependence on the morphology. To do this, we quantify the growth in stellar mass via star formation events of massive ($M > 10^{11}\,M_{\odot}$) galaxies as a function of size and brightness profile shape up to $z \sim 2$. We base our discussion on the characterization of the dust infrared (IR) emission of these systems, which is linked to the amount of recent star formation and/or the presence of obscured active galactic nuclei (AGNs). This IR-based study is complementary to the more classical approach to the characterization of the evolution of massive ellipticals based on rest-frame optical properties.

Throughout this paper, we use a cosmology with $H_0 = 70\ \mathrm{km\ s^{-1}\ Mpc^{-1}}$, $\Omega_{M=0.3}$, and $\Lambda = 0.7$. All magnitudes refer to the AB system. The results for stellar masses and star formation rates (SFRs) assume a Chabrier (2003) initial mass function (IMF) with $0.1\,M_{\odot} < M < 100\,M_{\odot}$.

2. DATA DESCRIPTION

2.1. *The Sample*

To analyze the star formation properties of the most massive galaxies as a function of morphology, we use the catalog of 831 K-band-selected massive galaxies ($M > 10^{11}\,M_{\odot}$) in the Palomar Observatory Wide-Field Infrared (POWIR)/DEEP-2 survey (Davis et al. 2003; Bundy et al. 2006; Conselice et al. 2008) for which Trujillo et al. (2007) provide redshifts, stellar masses, and structural parameters (sizes and Sérsic indices). These data, jointly with the Multiband Imaging Photometer for *Spitzer* (MIPS) fluxes measured in the observations carried our by the Far-Infrared Deep Extragalactic Legacy Survey (FIDEL) Program in the extended Groth strip (EGS), allow a detailed analysis of the star formation properties of the most massive galaxies as a function of morphology up to $z \sim 2$.

The sample is described in detail in Conselice et al. (2007) and Trujillo et al. (2007). Briefly, the K-band survey covers 2165 arcmin^2 in the EGS and has a depth $K = 22.5$ mag (5 σ). Only 710 arcmin^2 are covered simultaneously with the *Hubble Space Telescope* Advanced Camera for Surveys (*HST* ACS) v- and i-band imaging from the All-Wavelength Extended Groth Strip International Survey (AEGIS; Davis et al. 2007), so reliable structural parameters can only be measured for 831 galaxies within the entire POWIR/DEEP-2 survey in EGS. Half of those 831 galaxies have spectroscopic redshifts based on optical data obtained by the DEEP-2 Galaxy Redshift survey (Davis et al. 2003). Conselice et al. (2007) estimate photometric redshifts for the rest of the sources with an accuracy $\Delta z/(1+z) = 0.025$. The 831 galaxies with $M > 10^{11}\,M_{\odot}$ in the EGS lie in the redshift range $0.2 < z \lesssim 2$. Stellar masses were estimated by Bundy et al. (2005, 2006) using the exponential star formation models of Bruzual & Charlot (2003) with a Chabrier (2003) IMF and various ages, metallicities, and dust contents included. As shown by Conselice et al. (2007), typical uncertainties in the stellar masses are a factor of $\sim$2 (typical of any stellar population study; see, e.g., Pérez-González et al. 2003, 2008; Kauffmann et al. 2003; Papovich et al. 2006; Fontana et al. 2006). As discussed in detail in Conselice et al. (2007), this factor includes the effects of the photometric redshift uncertainties, the errors inherent to solution degeneracies, and the choices of the IMF and the stellar emission library. For example, using Maraston (2005) models (with an improved treatment of the thermally pulsing asymptotic giant branch [TP-AGB] stellar evolution phase) would produce a 20% (at most) systematic decrease in the mass estimations. Using a Salpeter (1955) IMF would increase the stellar masses by a constant factor of 0.25 dex.

Trujillo et al. (2007) estimated (circularized) half-light radius (r_e) and Sérsic (1968) indices (n) for all the galaxies in our sample. They used i-band *HST* ACS images to fit surface brightness profiles and divided the sample in disklike and spheroid-like galaxies according to the value of the Sérsic index. Ravindranath et al. (2004; see also Andredakis et al. 1995) demonstrated that nearby galaxies with $n < 2.5$ are mostly disks, while spheroids are characterized by high Sérsic indices, $n > 2.5$. They also performed simulations to check that the Sérsic index obtained from *HST* data can be used as a morphology indicator at $z > 0$. Trujillo et al. (2007) extended these simulations to prove that the structural parameters are robust against the effects introduced by K-corrections, AGN contamination, and surface brightness dimming.

For our sample, visual inspection of the ACS i-band images by one of the coauthors (I. T.) was used to classify the sample in four types: ellipticals/lenticulars, spirals, irregulars, and mergers. Comparing this visual classification with the one based on Sérsic indices, we find that the visually confirmed spheroids present $\langle n \rangle = 4.8 \pm 1.5$, and the rest of the sources have $\langle n \rangle = 1.7 \pm 1.7$. There is a 6% contamination of visually identified spheroids in the $n < 2.5$ sample, and a 20% contamination of visually identified disks in the $n > 2.5$ sample (comparable to the 5% and 19% contaminations in Ravindranath et al. [2004]). The fraction of interloper disks decreases to 7% at $n > 4$ and 4% at $n > 5$. A 4% contamination is typical of other works based on visual or quantitative morphological classifications such as Conselice et al. (2007) or Bundy et al. (2005). The visual test shows that the galaxies with $n > 4$ form a robust (almost uncontaminated) sample of spheroid-like sources, and $n < 2.5$ galaxies are mostly disks. Galaxies with $2.5 < n < 4$ are most probably spheroid-like galaxies with some contamination of S0 galaxies and early-type spirals.

2.2. *UV-to-MIR Photometric Properties of the Sample*

The positions of the 831 massive galaxies in the EGS were cross-correlated (using a 1″ search radius) with our own reduction and catalogs of the *Spitzer* Infrared Array Camera (IRAC) survey of the EGS. Using the same simulation method described in Pérez-González et al. (2008) we found that this catalog is 75% complete at $\sim$1.5 μJy ([3.6] = 23.5 mag), which corresponds to 8 σ detections. Our IRAC photometry is consistent with that published by Barmby et al. (2008) for the same data set (but their own reduction and cataloging) within 0.1 mag (typical absolute uncertainty of IRAC fluxes) for 75% of the sample, and within 1 σ error for virtually all sources.

We found IRAC counterparts down to [3.6] = 23 mag for all of the 831 galaxies in Trujillo et al.'s (2007) sample. For 151 sources (18% of the total), the IRAC sources were blended with nearby objects, but still resolved (the separation was larger than 1″). As described in detail in Appendix A of Pérez-González et al. (2008), for these sources we obtained multiwavelength photometry (including *Spitzer* fluxes) using a deblending algorithm based on the deconvolution of the IRAC and MIPS images. The method takes the known positions of the blended sources obtained from optical/NIR ground-based images and the point-spread functions (PSFs) for the different images and obtains separated fluxes for the blended sources (see also Grazian et al. 2006). The method relies on the moderate resolution of the IRAC images ($\sim$2″ FWHM; not that different from an optical ground-based image, but very stable), which allows the deblending of sources separated by more than $\sim$1″ (half of the FWHM). For the MIPS 24 μm images, the resolution is worse ($\sim$6″ FWHM),

but the IRAC data can be used to assign the most probable counterparts and help with the deblending. In any case, the main results in this paper (the MIPS detection fraction and the statistics of specific SFRs) remain virtually unchanged (less than 5% random changes at all redshifts) when we remove the 151 sources with blending problems.

We measured consistent aperture photometry in several UV, optical, NIR, and MIR bands with the method described in Pérez-González et al. (2008). The multiwavelength data set is outlined briefly in Villar et al. (2008) and will be characterized in detail in G. Barro et al. (2008, in preparation). More noticeably, our merged photometric catalog includes MIPS fluxes at 24 μm obtained from aperture photometry in the guaranteed time observer (GTO) and FIDEL survey (Second Data Release [DR2]) data in the AEGIS EGS field (Davis et al. 2007; Symeonidis et al. 2007). Following the same procedure described in Pérez-González et al. (2005, 2008), we used the DAOPHOT software package in IRAF[5] to detect sources (using a 3 σ detection cut above the local sky noise) in the MIPS images and measure aperture photometry with a PSF fitting method.

Based on simulations consisting of the creation and recovery of artificial sources in these images, we found that our 24 μm catalog of the EGS is 75% complete at 35 μJy (consistent with Papovich et al. [2004] and Treister et al. [2006]); $F(24) = 35$ μJy corresponds to $\sim$6 σ detections for the average sky noise in the FIDEL DR2 images. Our 24 μm catalogs are cut to 3 σ detections, which translate to the range 14–17 μJy, depending on the location on the sky due to small differences in exposure time and the effect of confusion (both presenting small spatial variations throughout the image). As done in Pérez-González et al. (2005), we tested the reliability of the MIPS detections by analyzing the probability of having a counterpart within the search radius (1″) in other optical/NIR (ground-based and IRAC) bands for a random position on the sky of the 24 μm image. Having a counterpart in three different bands within the EGS data set has a negligible probability (1.4%), so we conclude that (virtually) all the MIPS detections within our sample are not spurious. Figure 1 shows postage stamps and spectral energy distributions (SEDs) of two typical examples of disklike galaxies and two spheroid-like galaxies detected by MIPS at 24 μm (also one 70 μm detection included).

Using the measured MIPS 24 μm fluxes, the estimated 280 nm synthetic fluxes inter-/extrapolated in the SED fits, and the spectroscopic and photometric redshifts published by Trujillo et al. (2007), we obtained total (unobscured plus obscured) SFRs for each galaxy in the same way as explained in Pérez-González et al. (2008; see also Bell et al. 2005). Briefly, the MIR fluxes at rest-frame wavelengths longer than 5 μm are fitted to dust emission models (from several libraries), and the IR-based SFRs are obtained from integrated total IR (using the calibration in Kennicutt [1998]) and rest-frame 24 μm (see Alonso-Herrero et al. 2006a) luminosities from the fits (averaged through all template libraries). The IR-based (obscured) SFR is then added to the UV-based (unobscured) SFR to obtain the total SFR. As discussed in Pérez-González et al. (2008), total SFR estimates should be good within a factor of 2. The SFRs discussed in the following sections were estimated assuming a Chabrier (2003) IMF, obtained by dividing the results obtained with the calibrations in Kennicutt (1998; valid for a Salpeter [1955] IMF) by a factor of 1.8.

[5] IRAF is distributed by the National Optical Astronomy Observatory, which is operated by the Association of Universities for Research in Astronomy (AURA), Inc., under cooperative agreement with the National Science Foundation.

3. RESULTS AND DISCUSSION

3.1. *IR Emission of the Most Massive Galaxies at $z \lesssim 2$*

Figure 2 shows the location of the MIPS detections in a stellar mass–size diagram for massive galaxies as a function of the concentration index. Out of the 831 galaxies in Trujillo et al.'s (2007) sample of massive galaxies, 485 sources (58%) were classified as spheroid-like based on their high ($n > 2.5$) Sérsic (1968) indices, and 346 (42%) as disklike sources ($n \leq 2.5$). Among the disklike sources, 322 (93% of all disks) are detected by MIPS at 24 μm with a minimum flux $F(24) = 15$ μJy, and 137 galaxies are detected at 70 μm down to $F(70) = 0.5$ mJy. Among the spheroids, 297 galaxies (61% of the total) are detected at 24 μm down to $F(24) = 14$ μJy, and 84 sources are detected at 70 μm down to $F(70) = 0.7$ mJy. If we consider only the MIPS 5 σ detections (i.e., more statistically reliable sources, although our simulations reveal that all of our 3 σ 24 μm sources are reliable to the 99% level; see § 2.2), the MIPS detection fractions decrease to 92% for disky systems and 52% for spheroid-like sources.

Table 1 shows the total number of sources and MIPS detection fractions (for fluxes above the 3 σ level) as a function of redshift and morphology. We consider the results based on the morphological classification using the Sérsic indices and the direct visual inspection of the images. The MIPS detection fractions for $n \leq 2.5$ galaxies and visually identified disks are almost identical. Visually confirmed spheroids present fewer MIPS detections than the $n > 2.5$ sources, although the difference is small (<10%) and consistent with the 20% contamination of visually identified disks in the $n > 2.5$ sample, most of them having $2.5 < n < 4.0$ (see Fig. 3).

Figure 2 shows that there is basically no difference between the loci occupied by MIPS detected and undetected galaxies in the stellar mass–size plane. However, for spheroid-like objects at a given stellar mass, MIPS nondetections are smaller than IR-bright sources by a factor of $\sim$1.2 (see also Zirm et al. [2007] results at higher z). This suggests that early (i.e., $z > 2$) massive star formation events left even more compact remnants than starbursts taking place at $z < 2$, perhaps reflecting the higher density conditions of the primitive universe.

Figure 3 shows the MIPS 24 μm detection fractions as a function of structural parameters. This figure confirms the bias of the $n \leq 2.5$ sample toward galaxies with ongoing (possibly extended through the disk) star formation or harboring an IR-emitting AGN. Figure 3 demonstrates that virtually all (80%–90%) of the $n \leq 2.5$ galaxies are detected by MIPS at all redshifts and (almost) independently of the size of the galaxy. In contrast, the spheroid sample is biased toward more quiescent systems. There is still a nonnegligible fraction (6%) of galaxies classified as disky which fall below the MIPS detection limit or do not present any IR emission, i.e., they have low-level star formation, no dust, or are completely quiescent. According to Figure 3, most of them lie at $z > 1$ (59% of all disklike nondetections) and tend to have comparatively smaller sizes: the MIPS detection fraction decreases from 90% for disklike galaxies with $r_e \gtrsim 4$ kpc to 70%–80% for $r_e \lesssim 1.5$ kpc systems. All these sources present very red SEDs (see Fig. 4).

On the contrary, the spheroid-like sample includes at least 63% of "active" galaxies. Moreover, some more MIPS undetected spheroids may have some star formation activity or harbor an AGN, since some of the SEDs in the upper left panel of Figure 4 present a significant emission in the UV, probably arising from young stars. Most of these UV-bright galaxies lie at $z > 1$, and the MIPS 24 μm flux upper limits[6] are consistent with the MIR emission from a typical

[6] The flux upper limits at 70 μm have been omitted from Fig. 4 for clarity, given that very few sources are detected at this wavelength.

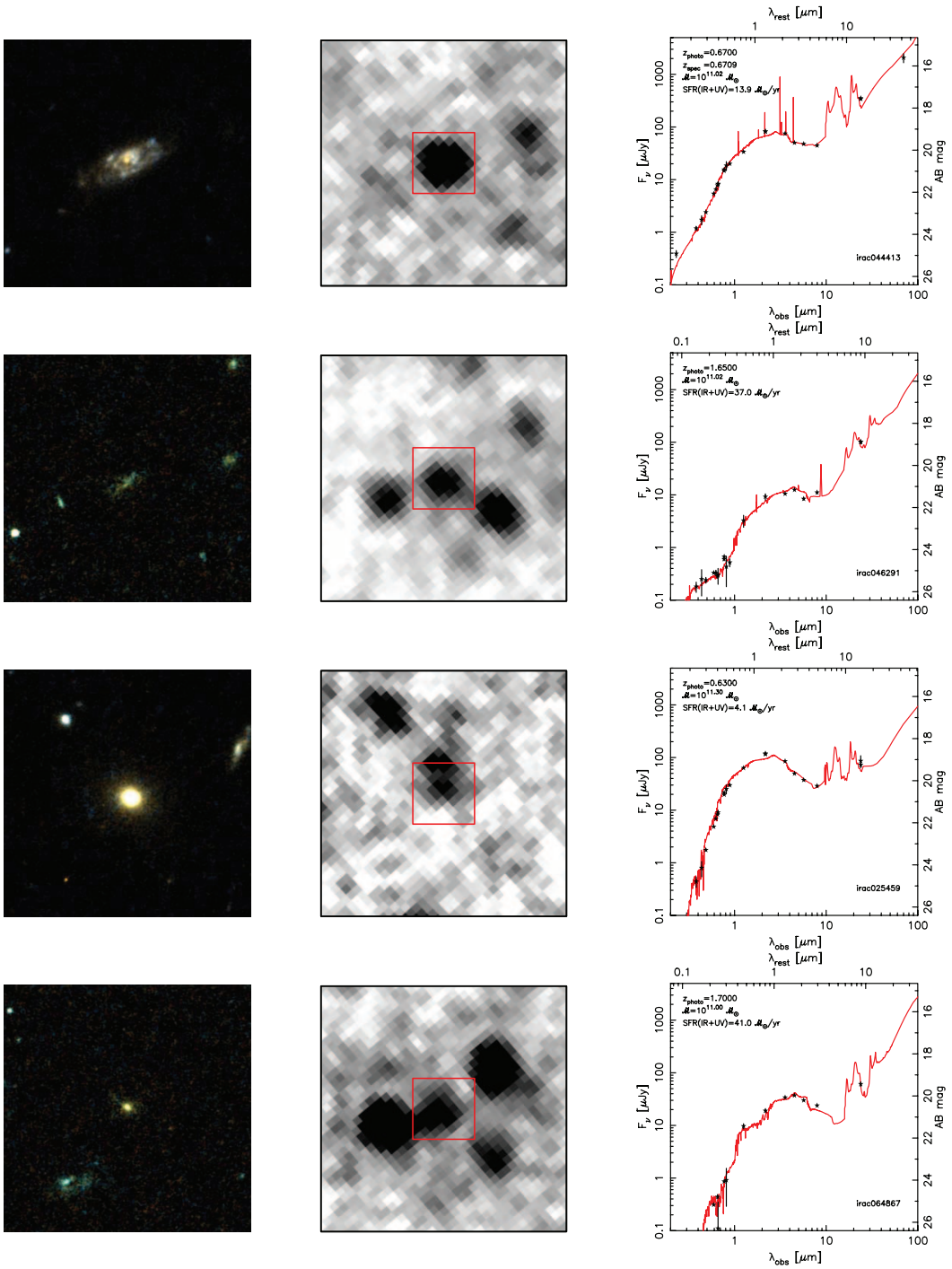

FIG. 1.—Postage stamps and SEDs for four typical MIPS detected galaxies in our sample of massive galaxies. Left panels show $10'' \times 10''$ RGB composite images built from *HST* ACS v and i frames. In the center column, MIPS 24 μm images of size $40'' \times 40''$ are depicted, with the red square showing the area covered by the ACS postage stamp. In all images, north is up and east is to the left. The right columns show the SEDs of each galaxy, fitted to stellar population and dust emission models which are used to estimate photometric redshifts, stellar masses, and SFRs (these parameters are given in each SED plot). The two upper rows show examples of disklike galaxies: EGS 142126.97+531137.4, a galaxy at $z = 0.67$; and EGS 142013.18+525925.0, lying at $z = 1.65$. The two lower rows show examples of spheroid-like galaxies: EGS 142021.47+525543.4, a galaxy at $z = 0.63$; and EGS 142125.76+531622.8, placed at $z = 1.70$.

Sc galaxy. Figure 3 shows that MIPS detections are more common among the largest spheroid-like galaxies, especially at $z > 1$. Interestingly, at $z > 1$ the MIPS detection fraction stays roughly constant at $r_e \lesssim 3$ kpc. It may even increase (up to 70%) for very compact ($r_e \lesssim 1$ kpc) spheroid-like galaxies, although there are three caveats to this result: (1) the number of sources with $r_e \lesssim 1$ kpc is small ($\sim$30), so the uncertainties in these bins are of order 20%–30%; (2) for $z > 1$ and $r_e \lesssim 1$ kpc we are reaching the resolution limit in the *HST* ACS images, and consequently the size measurements count with large uncertainties; and (3) these high-z compact galaxies may be dominated by an obscured AGN (since the galaxies are detected by MIPS and show no X-ray emission; see also Trujillo et al. 2007), which may bias the size measurements.

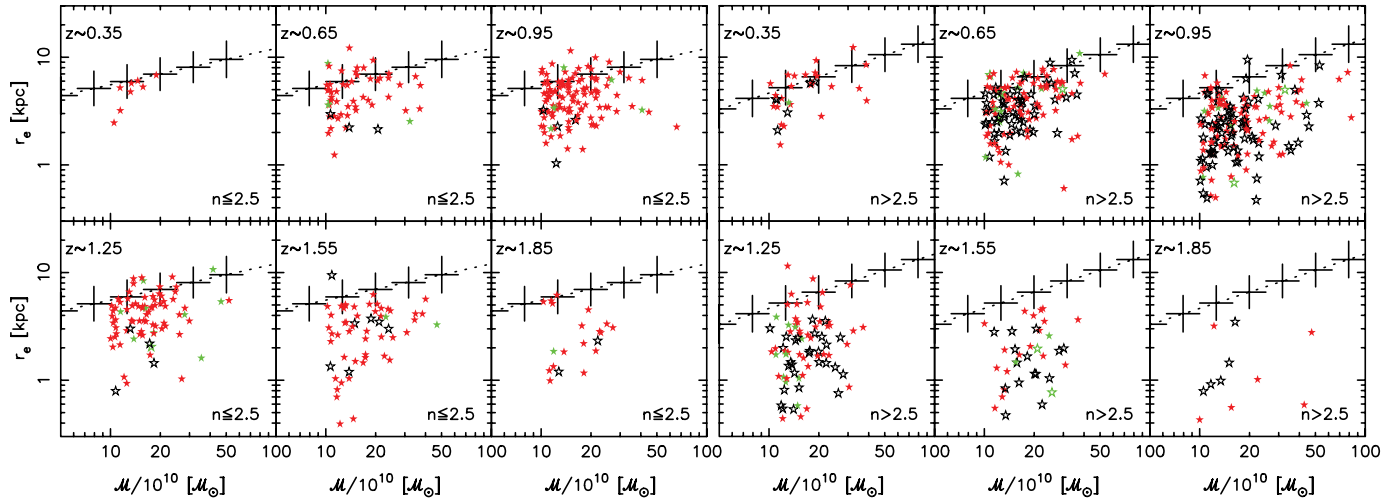

FIG. 2.—Stellar mass–size distribution for different redshift bins of our massive galaxies separated in disklike (*left panels*) and spheroid-like (*right panels*) types. Galaxies detected by MIPS at 24 μm are plotted with filled stars, while open stars show MIPS nondetections. Red symbols are galaxies whose MIPS emission is identified with obscured star formation, and green symbols depict galaxies which harbor an X-ray- or/and IR-emitting AGN.

Our results may be compared with those published by Rodighiero et al. (2007). They found that 20% of the most securely identified spheroids[7] at $0.3 < z < 1.0$ are detected during phases of prominent activity. The evidence is the detection at 24 μm above 80 μJy or at radio wavelengths above 40 μJy. Our MIPS data are deeper than theirs, but if we cut our catalogs to the same flux limit (see Fig. 3), we obtain an average ~20% detection fraction at $z < 1$ for the most concentrated objects with $n > 4$, probably well correlated with their sample of bona fide spheroids, although our selection only includes the most massive galaxies ($M > 10^{11}\ M_{\odot}$), and Rodighiero et al.'s selection is not based on stellar mass.

If we consider the high-z ($z > 1$) galaxies in our sample, our results are also consistent with those found in Papovich et al. (2006) for distant red galaxies (DRGs). These galaxies have a typical stellar mass $M \sim 10^{11}\ M_{\odot}$ and a mean redshift $z \sim 2$ (see also Grazian et al. 2007; Pérez-González et al. 2008). Given that our sample has a stellar mass cut $M > 10^{11}\ M_{\odot}$ and a redshift cut at $z = 2$, the low-redshift, high-mass tail of the general DRG population must be included in our selection. Indeed, we have 27 DRGs in our sample, with an average redshift $\langle z \rangle = 1.50 \pm 0.22$. Papovich et al. (2006) found that roughly 50% of DRGs are detected by MIPS at 24 μm down to 80 μJy. We find a ~60% detection fraction for massive galaxies in the low-redshift tail of DRGs ($1 < z < 2$) with deeper data (75% completeness level at 35 μJy). Among the 27 DRGs in our sample, 25 (93%) are detected by MIPS. This detection fraction is higher than the average for $1 < z < 2$ galaxies, but still consistent with the results in Papovich et al. (2006), who argue that $z \lesssim 2$ DRGs are mostly heavily extincted starbursts part of the class of dusty extremely red objects (EROs) at $z > 1$, and find a ~75% MIPS detection fraction for their $M > 10^{11}\ M_{\odot}$ DRGs at $z < 2$. Indeed, 18 DRGs in our sample are EROs (16 MIPS detections), and we count with a total of 305 EROs in our entire sample.

[7] Note that Rodighiero et al. (2007) cut their sample to clear E and E/S0 galaxies as classified visually by Bundy et al. (2005), but do not include Bundy's S0 type in their analysis.

3.2. *Spectral Energy Distributions*

Figure 4 shows the SEDs of all the massive galaxies in our EGS sample divided into morphological and activity types. The two panels on the right show the SEDs for galaxies with an X-ray detection (Barmby et al. 2006; Nandra et al. 2007; see also Conselice et al. 2007) or classified as IRAC power-law galaxies (PLGs; Alonzo-Herrero et al. 2006b; Donley et al. 2007), i.e., sources which most probably harbor an X-ray- and/or IR-emitting AGN. There are 68 X-ray emitters, 60 of them with MIPS detection, and five PLGs in total, all of them with X-ray emission and four with MIPS emission.

TABLE 1
MIPS DETECTION FRACTION AND SPECIFIC SFR STATISTICS AS A FUNCTION OF MORPHOLOGY

	SÉRSIC INDEX CLASSIFICATION				VISUAL CLASSIFICATION			
	Sources (MIPS Detected)[a]		log (SFR/M)[b]		Sources (MIPS Detected)[a]		log (SFR/M)[b]	
REDSHIFTS	$n \leq 2.5$	$n > 2.5$	$n \leq 2.5$	$n > 2.5$	S/Irr/mergers	E/S0	S/Irr/mergers	E/S0
(0.2, 0.5]	8 (100.0)	31 (80.6)	$-1.33^{-1.57}_{-1.08}$	$-2.03^{-2.23}_{-1.68}$	14 (100.0)	25 (76.0)	$-1.37^{-1.68}_{-1.12}$	$-2.12^{-2.36}_{-2.01}$
(0.5, 0.8]	55 (94.5)	144 (60.4)	$-1.05^{-1.34}_{-0.76}$	$-1.54^{-2.00}_{-1.22}$	88 (94.3)	111 (50.5)	$-1.12^{-1.43}_{-0.79}$	$-1.82^{-2.07}_{-1.46}$
(0.8, 1.1]	120 (95.8)	173 (57.2)	$-0.79^{-0.99}_{-0.62}$	$-1.59^{-1.81}_{-1.10}$	156 (95.5)	137 (48.2)	$-0.86^{-1.06}_{-0.63}$	$-1.63^{-1.86}_{-1.44}$
(1.1, 1.4]	83 (94.0)	83 (66.3)	$-0.60^{-0.76}_{-0.49}$	$-0.89^{-1.36}_{-0.66}$	104 (98.1)	62 (50.0)	$-0.63^{-0.83}_{-0.49}$	$-1.26^{-1.48}_{-0.90}$
(1.4, 1.7]	56 (87.5)	40 (57.5)	$-0.51^{-0.72}_{-0.30}$	$-0.61^{-1.07}_{-0.12}$	60 (86.7)	36 (52.9)	$-0.51^{-0.77}_{-0.23}$	$-0.61^{-0.98}_{-0.32}$
(1.7, 2.0]	21 (85.7)	12 (58.3)	$-0.17^{-0.50}_{+0.02}$	$-0.40^{-0.61}_{-0.13}$	24 (83.3)	9 (50.0)	$-0.36^{-0.61}_{+0.01}$	$-0.17^{-0.33}_{-0.06}$

[a] Values in parentheses in percent.
[b] In units of Gyr^{-1}.

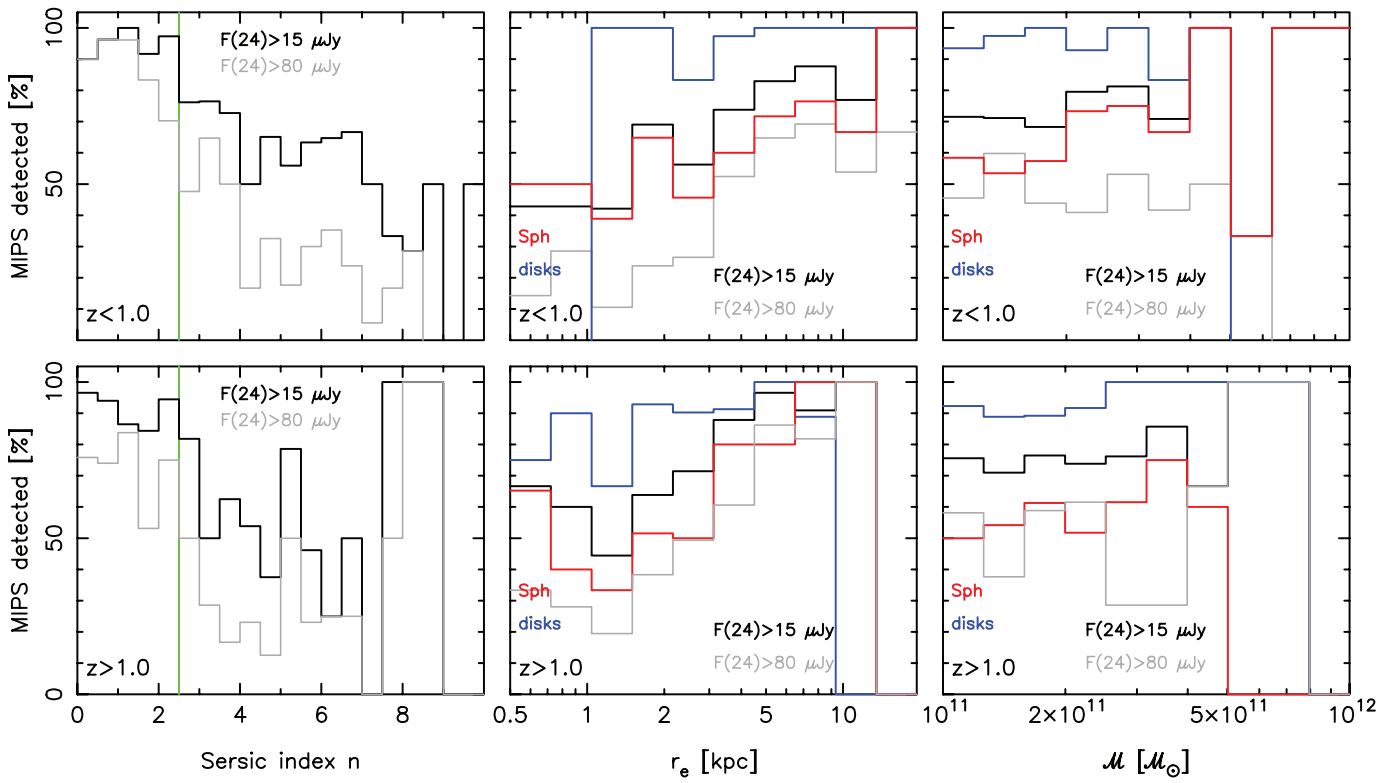

FIG. 3.—MIPS 24 μm detection fractions as a function of Sérsic index (*left panels*), (circularized) half-light radius (*center panels*), and stellar mass (*right panels*). The whole sample has been divided into two redshift intervals ($z < 1$ on the top panels, and $z > 1$ on the bottom panels). Galaxies identified as IR- or X-ray-bright AGNs are excluded from the distributions. In all plots, thick black lines show the results for all the MIPS detections [with a minimum measured value of $F(24) = 15$ μJy], and gray thin lines show the measured fractions for a flux cut $F(24) > 80$ μJy. In the left panels, the green vertical line shows the adopted separation between spheroid-like and disklike galaxies. In the center and right panels, red lines show the MIPS detection fractions for spheroid-like sources, and blue lines for disklike sources.

The SED distribution of the spheroids presents a lower scatter in the UV/optical, being very similar to a spectral template of an elliptical. In contrast, there is a very populated tail of disklike galaxies with UV/optical fluxes brighter than a template for a typical Sc galaxy, most probably linked to a recent starburst. The MIR emission is consistent with the PAH spectrum of a late-type spiral galaxy (see also Fig. 1), but can be as high as 6–10 times the flux of the Sc template from Polletta et al. (2007). Spheroid-like galaxies with a MIPS detection present a lower 24 μm median flux (82 μJy, with the quartiles being 42 and 188 μJy, and the average 160 μJy) than MIPS disky sources (190^{301}_{107} μJy, and the average 250 μJy). Most of the sources identified as AGNs present relatively bright fluxes at rest-frame wavelengths between 2 and 10 μm, revealing the presence of very hot dust heated by the central supermassive black hole and emitting in the NIR and MIR. In several cases, this NIR/MIR emission hides the 1.6 μm bump, typically seen in galaxies whose spectrum is dominated by stars rather than dust.

3.3. *Specific Star Formation Rates*

Figure 5 shows the specific SFRs of massive galaxies as a function of redshift and morphology. Table 1 gives the median and quartiles for different redshift ranges and morphological types (obtained from Sérsic index and visual classifications). The median specific SFRs increase by less than 0.1 and 0.02 dex for spheroids and disks, respectively, when considering MIPS 24 μm detected above the 5 σ level. These increments do not affect the following results significantly.

When segregating the sample based on the Sérsic indices, we find that the specific SFRs of spheroid galaxies evolve as $(1+z)^{5.5\pm0.6}$ from $z = 0$ to $z = 2$, while the evolution for disk-like galaxies goes as $(1+z)^{3.6\pm0.3}$. If we consider the results based on the visual classification, the evolution is more pronounced for spheroids and almost identical for disks: $(1+z)^{6.4\pm0.8}$ evolution for the former, and $(1+z)^{3.4\pm0.2}$ for the latter.

The specific SFRs used in Figure 5 have been estimated by adding the unobscured SFRs obtained from UV data (at rest frame 280 nm) and the obscured SFRs from IR data (using the total IR luminosity), as explained in Pérez-González et al. (2008). The ratio between these two quantities allows the estimation of the global obscuration of the recent star formation in each galaxy (only for those detected by MIPS). On average, we find that extinctions for MIPS detected galaxies increase with redshift, ranging from $\langle A(V)\rangle = 1.0 \pm 0.5$ mag at $z < 0.5$ to $\langle A(V)\rangle = 1.5 \pm 0.6$ mag at $z \sim 1$, and $\langle A(V)\rangle = 2.0 \pm 0.7$ mag at $z \sim 2$. These values are consistent with typical attenuations found for IR-bright galaxies by, e.g., Rigopoulou et al. (2000) and the evolution in the extinction properties of the UV SFR density found by Tresse et al. (2007). According to Symeonidis et al. (2007), even larger extinctions (up to a factor of ~100) are needed to match SFRs obtained from IR or radio data and SFRs obtained from [O II] spectroscopic observations of IR-bright sources in the EGS.

Figure 5 shows that below $z = 1.1$ spheroid-like galaxies present very low specific SFRs. On average, they would increase their stellar mass by less than 25% at $0 < z < 1$ if they maintained a constant SFR. The global mass increase (in the form of newly formed stars) for all spheroid-like galaxies is less than 10% if we take into account the 38% of $z < 1$ spheroids which are not detected by MIPS, and even lower (~5%) if we only consider the visually identified spheroids. In contrast, disklike galaxies could typically double their mass from $z = 1$ to $z = 0$ due to newly formed stars if they maintained a constant SFR, with little change

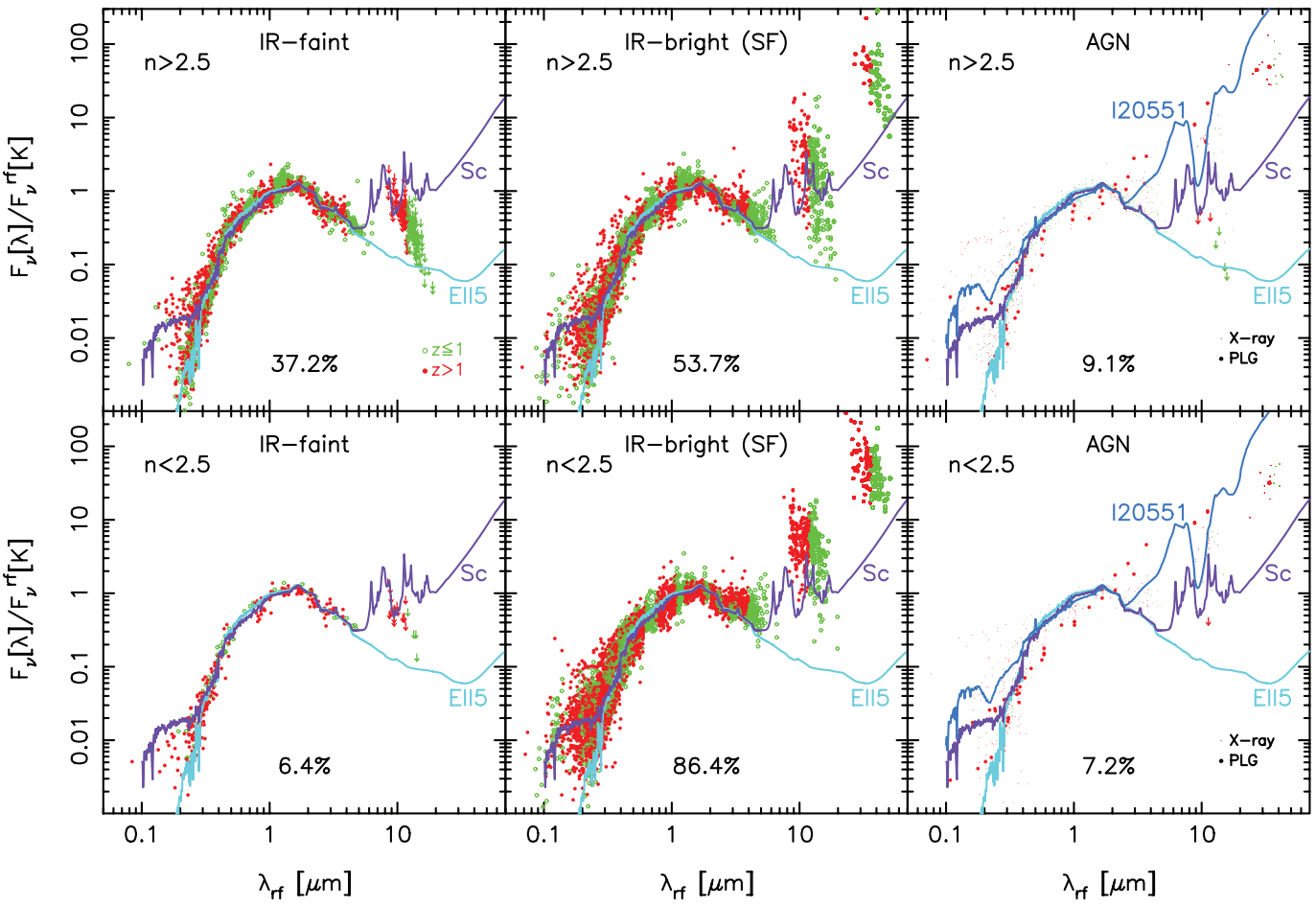

FIG. 4.— SEDs (deredshifted and normalized to the rest-frame *K*-band flux) of all the galaxies in the sample of massive galaxies ($M > 10^{11}\ M_\odot$) in the EGS (Trujillo et al. 2007). The upper and lower panels show the SEDs for the spheroid-like and disklike galaxies, respectively. For each morphological type, the subsample has been divided into three groups: galaxies without MIPS detection (IR-faint, *left panels*, with arrows showing an upper limit of the MIPS 24 μm emission corresponding to 15 μJy, the minimum flux observed in the sample), galaxies with a MIPS counterpart most probably linked to ongoing star formation (IR-bright, *center panels*), and galaxies with nuclear activity (AGNs; *right panels*; see text for details). In each panel, open green circles show sources at $z < 1$, and filled red circles depict galaxies at $1 < z < 2$. We also show typical templates (from Polletta et al. 2007) of an elliptical galaxy (Ell5), a late-type spiral galaxy (Sc), and a galaxy with an obscured AGN (I2 0551; just for the AGN panels on the right). All panels show the fraction of sources in each type for the spheroid-like and disklike samples.

due to the very few galaxies (less than 5%) for which we only have SFR upper limits.

In practice, IR-bright intense star-forming bursts are not expected to last long (Mihos & Hernquist 1994), so a galaxy most probably will not maintain a high SFR level for several gigayears. The higher SFR values are expected to be maintained for shorter periods, since gas exhaustion and supernova winds (and even AGN activity) will help to suppress star formation. Mihos & Hernquist (1996) simulations of mergers predict the triggering of a very intense and short starburst event (probably detectable in the MIR by MIPS) lasting a few tens of megayears (and occurring in late stages of the merger, when the galaxies are actually joining) for encounters of galaxies with an already formed bulge. Encounters of disky galaxies would trigger less intense bursts lasting longer (100–200 Myr) and occurring earlier in the merger process. For the observed specific SFRs in our sample, those short and intense starbursts would add up to less than 0.01% (for each merging event) to the total stellar mass of a typical spheroid-like galaxy at $z < 1$. This very small fraction of young stars would be hidden by the predominant old stellar population and be undetectable in local ellipticals. For the disky galaxies at $z < 1$, which present specific SFRs as high as 0.2 Gyr^{-1}, the burst strength (ratio of the newly formed stars to the global stellar mass) could be as high as a few percent (for each merging event), typical for star-forming galaxies at low redshifts (Kauffmann et al. 2003; Pérez-González et al. 2003).

At $z \gtrsim 1$, the specific SFRs of massive galaxies are higher than 0.1 Gyr^{-1}, both the active spheroid-like (note that there are 40% of spheroids which are not detected by MIPS) and disky systems are forming stars at approximately the same rate, and the number of quiescent galaxies (those not detected by MIPS) is less than ~50% for both types. It is interesting to note that most galaxies (disks and spheroids) have significant amounts of dust, since they are detected at 24 μm. If some of these galaxies are the progenitors of nearby ellipticals, that dust should have disappeared somehow, or it is now very cold and may only be detected at very long wavelengths ($\lambda > 100$–200 μm) and low fluxes.

For typical burst durations, and even for star-forming events with a constant SFR and lasting up to 1 Gyr, the maximum increase in stellar mass would be ~15% at $1.1 < z < 1.4$, ~25% at $1.4 < z < 1.7$, and ~50% at $1.7 < z < 2.0$, for both spheroids and disks. This means that a significant fraction (more than 50%) of the stellar mass of $z > 1$ massive galaxies was assembled at $z > 2$ (Pérez-González et al. 2008; see also Bauer et al. 2005; Feulner et al. 2005; Papovich et al. 2006). Moreover, we find that about 40% of spheroids at $z \sim 1.8$ are almost "dead" (they present low SFR levels based on IR and UV data) and evolving passively, or may be experiencing a quiescent period. Note that most

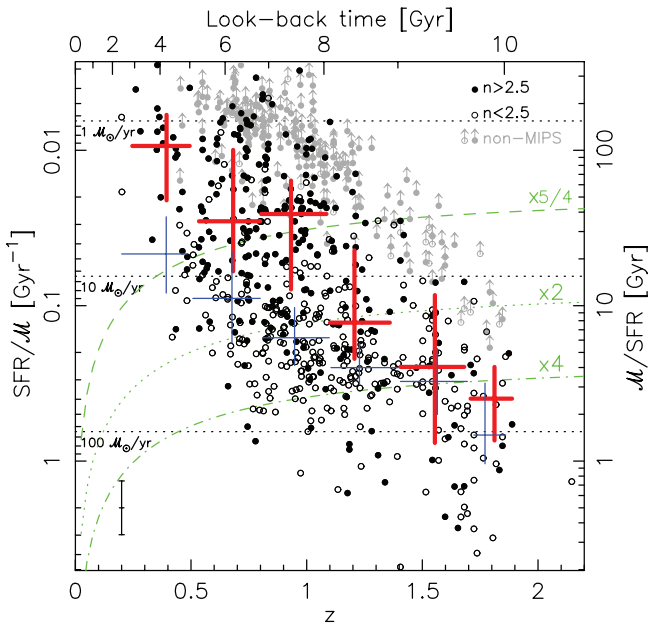

FIG. 5.—Specific SFRs as a function of redshift and morphology (for galaxies not identified as bright AGNs). Galaxies detected at 24 μm are plotted with open (disks) and filled (spheroids) black circles, while gray symbols show upper limits for sources not detected by MIPS. Red and blue plus signs represent the median and quartiles for the distribution of specific SFRs in the different redshift ranges used in Trujillo et al. (2007; with red thickest lines referring to spheroids and blue thinnest to disky galaxies). Green curves show the expected positions of galaxies which would multiply their stellar mass by 5/4, 2, and 4 between their redshift and $z = 0$ if they maintained a constant SFR. Horizontal dashed lines show constant SFR values for the median stellar mass of our sample ($1.6 \times 10^{11}\ M_\odot$).

spheroid-like galaxies at $z > 1$ would be qualified as passive based on optical colors alone, but the MIPS data reveal that ~50% of them are experiencing dusty starbursts and 10% more harbor (also) obscured AGNs.

We can estimate how much stellar mass galaxies typically assemble through star formation from $z = 2$ to the present (i.e., the star formation efficiency to increase the mass of a galaxy in the last 10 Gyr) if a galaxy follows the specific SFR evolution depicted in Figure 5. We assume that the SFRs remain constant within each redshift interval; since the starbursts probably last 50–200 Myr, as discussed earlier, the following figures would be an upper limit. Adding all the mass formed from $z = 2$ to $z \sim 0$, we estimate that a disklike galaxy could increase its stellar mass by up to a factor of 3.2 ± 0.5 in the last 10 Gyr: 1.4 times increase at $1.7 < z < 2.0$, and an almost constant 10%–20% increase in each of our five redshift intervals at $z < 1.7$. A spheroid-like galaxy could increase its stellar mass by up to a factor of 1.8 ± 0.3 : 1.2 times increase at $1.7 < z < 2.0$, 10%–20% in each of our two intervals at $1.1 < z < 1.7$, and less than 5% in each of the three intervals at $z < 1.1$. These figures are almost unchanged (<5% increases) when considering only the MIPS 24 μm 5 σ detections. For visually identified disks and spheroids, the stellar mass increases by up to a factor of 2.7 ± 0.4 and 1.8 ± 0.3, respectively.

Ideally, one would like to disentangle what is the relative contribution to the size growth of a galaxy of newly formed stars and system heating through merger/interactions. However, both processes are probably linked, since new star formation events are likely associated to the interactions that could inject energy to the systems. Consequently, a definitive answer to the problem of how galaxies grow requires the help of elaborate modeling. It is worth saying, nonetheless, that both the observations at low- and high-z show that galaxies have larger effective radii when observed in bluer bands. This means that younger stars are preferentially located at larger galactocentric distances than older populations. In this paper, we have quantified how much the stellar mass grows through star formation events only. Once we reach a clear picture of how the galaxies can increase in size through mergers, our results will constrain the amount of stellar mass due to dry accretion that is necessary to migrate the high-z galaxies to the local size-mass relations.

4. SUMMARY AND CONCLUSIONS

We have analyzed the stellar mass growth in the form of newly born stars in a sample of 831 K-band-selected massive galaxies ($M > 10^{11}\ M_\odot$) as a function of structural parameters (size and concentration). These galaxies lie in the redshift range between $z = 0.2$ and $z \sim 2$. Our analysis is based on the measurement of the specific SFR for each galaxy based on their UV and IR emission, taking advantage of the deep *Spitzer* data obtained by the FIDEL *Spitzer* MIPS Legacy Project in the extended Groth strip.

Our main results follow:

1. Most (more than 85% at any redshift) disklike galaxies (identified by small Sérsic indices; $n < 2.5$) are detected by MIPS at 24 μm down to $F(24) = 15$ μJy with a median flux $F(24) = 190$ μJy.
2. A significant fraction (more than 55% at any redshift) of spheroid-like galaxies is detected at 24 μm down to $F(24) = 14$ μJy with a median flux $F(24) = 82$ μJy.
3. The MIPS detection fraction for spheroid-like galaxies is higher (70%–90%) for larger ($r_e \gtrsim 5$ kpc) galaxies, especially at $z > 1$, where the detection fraction has a minimum around 30%–40% for galaxies with $r_e \sim 1$ kpc. No clear trend is found for disky galaxies of different sizes.
4. There is basically no difference between the loci occupied by MIPS detected and undetected galaxies in the stellar mass–size plane. However, for spheroid-like objects at a given stellar mass, MIPS nondetections are smaller than IR-bright sources by a factor of ~1.2.
5. Most of the galaxies in our sample present spectral energy distributions which are consistent with an elliptical template in the UV/optical/NIR spectral range. Some galaxies morphologically classified as spheroids have UV emission tails which are typical of star-forming systems, most commonly at $z > 1$.
6. A ~10% fraction of the massive galaxies in our sample present X-ray or power-law-like MIR emission which must be linked to the presence of a bright (unobscured or obscured) AGN.
7. Based on the measured specific SFRs, we estimate that spheroid-like galaxies have doubled (at the most, depending on the burst durations) their stellar mass due to newly born stars alone from $z \sim 2$ to $z = 0.2$. Most of these mass increases (60%) occur at $z \gtrsim 1$, where specific SFRs are as high as 0.4 Gyr^{-1}.
8. Disklike galaxies have tripled (at the most) their stellar mass by newly formed stars at $z < 2$, with a more steady growth rate as a function of redshift.

We thank an anonymous referee for her/his very constructive comments. We acknowledge support from the Spanish Programa Nacional de Astronomía y Astrofísica under grants AYA 2006-02358 and AYA 2006-15698-C02-02. This work is based in part on observations made with the *Spitzer Space Telescope*, which is operated by the Jet Propulsion Laboratory, Caltech under NASA contract 1407. P. G. P.-G. and I. T. acknowledge support from the Ramón y Cajal Program financed by the Spanish Government and the European Union.

REFERENCES

Alonso-Herrero, A., Rieke, G. H., Rieke, M. J., Colina, L., Pérez-González, P. G., & Ryder, S. D. 2006a, ApJ, 650, 835
Alonso-Herrero, A., et al. 2006b, ApJ, 640, 167
Andredakis, Y. C., Peletier, R. F., & Balcells, M. 1995, MNRAS, 275, 874
Arnouts, S., et al. 2007, A&A, 476, 137
Barmby, P., Huang, J.-S., Ashby, M. L. N., Eisenhardt, P. R. M., Fazio, G. G., & Wright, E. L. 2008, ApJS, 177, 431
Barmby, P., et al. 2006, ApJ, 642, 126
Bauer, A. E., Drory, N., Hill, G. J., & Feulner, G. 2005, ApJ, 621, L89
Baugh, C. M., Cole, S., & Frenk, C. S. 1996, MNRAS, 283, 1361
Bell, E. F., et al. 2005, ApJ, 625, 23
Boylan-Kolchin, M., Ma, C.-P., & Quataert, E. 2006, MNRAS, 369, 1081
Bruzual, G., & Charlot, S. 2003, MNRAS, 344, 1000
Bundy, K., Ellis, R. S., & Conselice, C. J. 2005, ApJ, 625, 621
Bundy, K., et al. 2006, ApJ, 651, 120
Chabrier, G. 2003, ApJ, 586, L133
Cimatti, A., et al. 2008, A&A, 482, 21
Cole, S., Lacey, C. G., Baugh, C. M., & Frenk, C. S. 2000, MNRAS, 319, 168
Conselice, C. J., Bundy, K., U, V., Eisenhardt, P., Lotz, J., & Newman, J. 2008, MNRAS, 383, 1366
Conselice, C. J., et al. 2007, MNRAS, 381, 962
Cowie, L. L., Songaila, A., Hu, E. M., & Cohen, J. G. 1996, AJ, 112, 839
Daddi, E., Cimatti, A., Renzini, A., Fontana, A., Mignoli, M., Pozzetti, L., Tozzi, P., & Zamorani, G. 2004, ApJ, 617, 746
Daddi, E., et al. 2005, ApJ, 626, 680
Davis, M., et al. 2003, Proc. SPIE, 4834, 161
———. 2007, ApJ, 660, L1
De Lucia, G., Springel, V., White, S. D. M., Croton, D., & Kauffmann, G. 2006, MNRAS, 366, 499
Donley, J. L., Rieke, G. H., Pérez-González, P. G., Rigby, J. R., & Alonso-Herrero, A. 2007, ApJ, 660, 167
Elston, R., Rieke, G. H., & Rieke, M. J. 1988, ApJ, 331, L77
Feulner, G., Gabasch, A., Salvato, M., Drory, N., Hopp, U., & Bender, R. 2005, ApJ, 633, L9
Fontana, A., et al. 2006, A&A, 459, 745
Franx, M., et al. 2003, ApJ, 587, L79
Gallazzi, A., Charlot, S., Brinchmann, J., & White, S. D. M. 2006, MNRAS, 370, 1106
Glazebrook, K., et al. 2004, Nature, 430, 181
Grazian, A., et al. 2006, A&A, 449, 951
———. 2007, A&A, 465, 393
Heavens, A., Panter, B., Jimenez, R., & Dunlop, J. 2004, Nature, 428, 625
Hughes, D. H., et al. 1998, Nature, 394, 241
Jimenez, R., Bernardi, M., Haiman, Z., Panter, B., & Heavens, A. F. 2007, ApJ, 669, 947
Juneau, S., et al. 2005, ApJ, 619, L135
Kauffmann, G., et al. 2003, MNRAS, 341, 33
Kennicutt, R. C. 1998, ARA&A, 36, 189
Kriek, M., et al. 2008, ApJ, 677, 219
———. 2006, ApJ, 649, L71
Labbé, I., et al. 2007, ApJ, 665, 944
Longhetti, M., et al. 2007, MNRAS, 374, 614
Maraston, C. 2005, MNRAS, 362, 799
Mihos, J. C., & Hernquist, L. 1994, ApJ, 431, L9
———. 1996, ApJ, 464, 641
Naab, T., Johansson, P. H., Ostriker, J. P., & Efstathiou, G. 2007, ApJ, 658, 710
Nandra, K., et al. 2007, ApJ, 660, L11
Papovich, C., et al. 2004, ApJS, 154, 70
———. 2006, ApJ, 640, 92
Pérez-González, P. G., Gil de Paz, A., Zamorano, J., Gallego, J., Alonso-Herrero, A., & Aragón-Salamanca, A. 2003, MNRAS, 338, 525
Pérez-González, P. G., et al. 2005, ApJ, 630, 82
———. 2008, ApJ, 675, 234
Polletta, M., et al. 2007, ApJ, 663, 81
Ravindranath, S., et al. 2004, ApJ, 604, L9
Reddy, N. A., Erb, D. K., Steidel, C. C., Shapley, A. E., Adelberger, K. L., & Pettini, M. 2005, ApJ, 633, 748
Rigopoulou, D., et al. 2000, ApJ, 537, L85
Rodighiero, G., et al. 2007, MNRAS, 376, 416
Salpeter, E. E. 1955, ApJ, 121, 161
Sánchez-Blázquez, P., Gorgas, J., Cardiel, N., & González, J. J. 2006, A&A, 457, 809
Sérsic, J. L. 1968, Atlas de Galaxias Australes (Cordoba: Obs. Astron.)
Springel, V., et al. 2005, Nature, 435, 629
Symeonidis, M., et al. 2007, ApJ, 660, L73
Toft, S., et al. 2007, ApJ, 671, 285
Treister, E., et al. 2006, ApJ, 640, 603
Tresse, L., et al. 2007, A&A, 472, 403
Trujillo, I., Conselice, C. J., Bundy, K., Cooper, M. C., Eisenhardt, P., & Ellis, R. S. 2007, MNRAS, 382, 109
Trujillo, I., et al. 2006, MNRAS, 373, L36
van Dokkum, P. G., et al. 2008, ApJ, 677, L5
Villar, V., Gallego, J., Pérez-González, P. G., Pascual, S., Noeske, K., Koo, D. C., Barro, G., & Zamorano, J. 2008, ApJ, 677, 169
Zirm, A. W., et al. 2007, ApJ, 656, 66